Progress In Electromagnetics Research C, Vol. 104, 13–24, 2020

E-Shape Microstrip Antenna for Dual Frequency WLAN Application

Aarti G. Ambekar and Amit A. Deshmukh

Abstract—For exploring the possibility of dual frequency response, a higher order mode frequency response in the air suspended design of a wideband E-shape microstrip antenna is studied by appropriately decreasing the air gap. The decrease in the air gap realizes the impedance matching at higher order TM_{12} mode which, along with the fundamental TM_{10} mode, gives dual frequency response. On an air suspended FR4 substrate with total thickness of $0.043\lambda_g$ optimized single patch configuration yields dual band response at 2427 and 5730 MHz giving frequency ratio of 1 : 2.36. It yields impedance bandwidths of 6.6% and 4.8% at two frequencies with respective broadside gains of 6.8 and 2.1 dBi. The proposed configuration satisfies the requirements of 2.4/5.8 GHz WLAN applications. Parametric formulations are proposed for various antenna dimensions. The MSAs redesigned using them at given fundamental mode frequency yield a similar dual band response.

1. INTRODUCTION

A wireless local area network (WLAN) is one of the wireless communication applications used for providing access between the client devices. According to the IEEE standard WLAN network covers 2.4 GHz (802.11 b/g) and 5–5.8 GHz (802.11a) frequency bands. A microstrip antenna (MSA) can be the best choice for such applications due to its light weight, low profile, and ease of integration with other peripheral devices. But MSAs suffer from the problem of narrow bandwidth (BW) and low gain. In order to satisfy the need of WLAN standards, the design of a dual band MSA with enhanced BW, gain, and similar radiation characteristics in two bands giving frequency ratio of 1 : 2–2.4 is essential. A few approaches like using thicker substrate, introducing parasitic elements, or modifying patch geometry by embedding a slot can be used for BW enhancement [1–4]. Here the slot cut technique is preferably used, and the best examples are U-slot, E-shape, and V-slot cut MSAs [5–10]. A dual frequency MSA for WLAN application using arc shape slots has been reported in [11]. But here the realized BW is less although the design is fabricated on an electrically thicker substrate. The design using a organic magnetic material substrate makes the configuration complex [12] while the design reported in [13] lacks explanations for antenna working in terms of patch modes with respect to the slot dimensions. Owing to the multiple patch parameters and feeding method multiband designs as reported in [14, 15] are complex in implementation. Designs of dual band rectangular MSA (RMSA) embedded with two pairs of rectangular slots and a shorting pin [16], an asymmetric M-shape antenna derived from E-shape patch using shorting vias at one of the arms [17] and a single feed MSA using a rectangular loop and an E-shape patch with shorting pin [18] lack in-depth explanation about antenna working in terms of patch modes with respect to shorting vias and the embedded slots. Biasing circuits used for active devices make the reconfigurable antennas reported in [19, 20] more complex in implementation. Nonuniform square ring geometry for dual band operation has been reported in [21]. But here BW realized is 2.5% though it is fabricated using two layers. Multiple patches have been used for the realization of dual band response in [22], but it increases the total patch size.

Received 2 June 2020, Accepted 9 July 2020, Scheduled 18 July 2020
* Corresponding author: Aarti G. Ambekar (arti1910@gmail.com).
The authors are with the EXTC Department, SVKM's DJSCE, Mumbai, India.

In this paper, initially the wideband design of coaxially fed E-shape MSA is discussed which yields BW of 442 MHz (18%). Further to explore the dual band nature of wideband E-shape patch, the higher order mode frequency response of the wideband configuration is studied. Because of the electrically thicker substrate in the wideband design at higher order mode frequencies, impedance matching at them is not realized. Further, a parametric study was carried out for the decrease in the air gap in the suspended wideband design to explore the possibility of impedance matching at higher frequencies. For a substrate of thickness less than $0.045\lambda_g$ impedance matching at lower and higher order modes together is obtained. Parametric study was carried out further to study the effects of slots in an E-shape patch on the resonant modes in achieving this dual band response. It is revealed that the dual frequency behavior was due to the patch TM_{10} and modified TM_{12} resonant modes. An optimum response with two frequencies at 2427 and 5730 MHz with BWs of 6.6 and 4.8% is obtained. This yields a ratio of 1 : 2.36 amongst the two frequencies. A broadside radiation pattern with peak gains of 6.8 and 2.1 dBi is observed in lower and higher frequency bands. As a design methodology, parametric formulation for the redesigning of similar dual band E-shape MSA is presented. The antennas designed using those yield a similar dual band response with frequency ratio around 1 : 24. Thus, the originality in the present work lies in providing in depth explanation for the realization of dual band response by investigating the higher order mode excitation in the traditional coaxially fed E-shape MSA. The dual frequency response with said frequency ratio is obtained on an electrically thinner substrate. Also no structural modifications in original E-shape MSA are needed, and thus the proposed design is simpler in implementation than the reported dual band MSAs. Detailed comparison highlighting the same is presented further in the paper. The proposed antenna is first analyzed using CST simulation software [23]. In simulation and measurements, a square ground plane of side length 10 cm is used. An SMA panel type connector is used to feed the antenna. High frequency instruments, namely ZVH — 8, FSC 6 and SMB — 100 A were used for the experimental verification. A good agreement is obtained between the simulated and measured results.

2. DUAL BAND E-SHAPE MSA

E-shape MSA is a widely reported design for realizing wideband response. Using the coaxial feed, MSA is optimized on an electrically thicker substrate ($0.06 - 0.08\lambda_g$). In the reported literature on suspended wideband E-shape MSAs and their variations, neither the impedance matching considerations have been discussed for realizing dual or multi-band frequency response with respect to patch higher order resonant modes nor the current distributions at those modes were studied to get the desired pattern characteristics. Therefore in the present paper, initially higher order mode frequency response of wideband E-shape patch is studied for achieving the desired impedance matching for getting the possible dual band response. Initially, wideband E-shape MSA design is parametrically optimized for the BW in the lower frequency band (i.e., 2400 MHz) of WLAN application. The E-shape MSA for the same is shown in Figs. 1(a), (b). Throughout the paper, patch dimensions and frequencies are referred in 'cm' and 'MHz', respectively. The E-shape patch is fabricated on an FR4 substrate ($\varepsilon_r = 4.3$, $\tan\delta = 0.02$, $h = 0.16$ cm), and it is suspended above the ground plane using an air gap (h_a) of 0.64 cm. The equivalent RMSA dimensions are 'L' = 4.2 and 'W' = 5 cm, which give fundamental TM_{10} mode frequency of 2435 MHz. Thus with reference to this frequency electrical substrate thickness is $0.066\lambda_g$. The MSA is coaxially fed using an SMA panel type connector with an inner probe diameter of 0.12 cm at 'X_f' = 1.0 and 'Y_f' = 0 cm. Due to the optimum separation between TM_{10} and TM_{02} resonant modes, broadband response with a BW of 442 MHz (18%) is obtained in E-shape MSA, as shown in Fig. 1(c). Further, wideband E-shape MSA is simulated for frequencies up to 7000 MHz, and respective input impedance plot is shown in Fig. 1(c). As can be seen, an impedance matching for VSWR less than 2 is not obtained for higher order resonant modes. With respect to the higher order mode frequency (5385 MHz), the electrical substrate thickness is in excess of $0.15\lambda_g$, which makes the impedance locus highly inductive. Therefore, the impedance mismatch is attributed to the higher value of '$(h_a + h)/\lambda_g$' at higher frequencies. In order to reduce this inductance in the impedance locus and to exploit the possibility of dual band response with reference to the higher order resonant modes, a parametric study is carried out for variations in air gap 'h_a', and the corresponding input impedance plots are provided in Figs. 1(c), (d). For 'h_a' = 0.64 cm, a loop lies inside VSWR = 2 circle which is

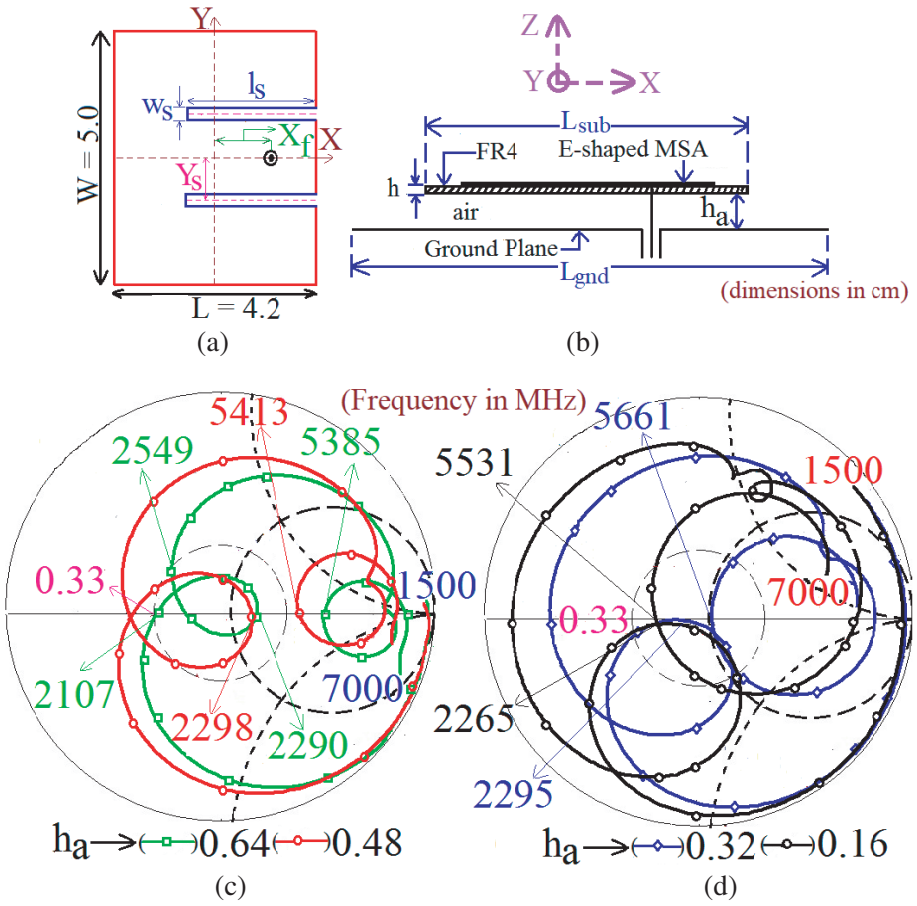

Figure 1. (a) Top and (b) side views of E-shape MSA, $L_{sub} = 6$, $W_{sub} = 7$, $L_{gnd} = W_{gnd} = 10$ cm, and its (c), (d) impedance plots for air gap 'h_a' variations in the suspended design.

attributed to the optimized broadband response with reference to the fundamental resonant mode. One more loop lies outside VSWR = 2 circle which is attributed to the improper impedance matching at the higher order mode. With decrement in the air gap 'h_a', the inductive component in the impedance locus decreases which makes the locus shift towards the lower resistance as well as larger capacitive region in the Smith chart. For air gap less than 0.32 cm, impedance locus due to fundamental as well as higher order modes lies inside VSWR = 2 circle. An optimum response in terms of range of frequencies lying inside VSWR = 2 circle at fundamental and higher order modes is observed for 'h_a' = 0.32 cm. With reference to the TM_{10} mode frequency of the patch, this thickness corresponds to the total substrate thickness ($h_a + h$) of around $0.043\lambda_g$. Therefore, this suspended variation with air gap of 0.32 cm is further studied for achieving the dual band response with reference to the fundamental and higher order resonant modes. For this a systematic parametric study for variation in the feed point location and pair of slot length increments is carried out to ascertain the resonant modes involved in the dual frequency response as well as the radiation pattern present in the two bands.

The design is initiated with a simple rectangular patch with dimensions 'L'= 4.2 and 'W' = 5.0 cm for which fundamental mode frequency (f_{TM10}) is 2435 MHz. Initially the parametric variations are carried for the feed position 'X_f', and corresponding resonance curve plots are as shown in Fig. 2(a). The feed variation is studied here since the excitation of various resonant modes is a function of the same. For 'X_f' = 1 cm, five resonant peaks are observed. In RMSA, TM_{mn} modes are present, where 'm' and 'n' indicate the number of half wavelength variations along the patch length and width [2]. In the current plots obtained using simulation software, current vector originates from the point where the field has '+' polarity and terminates at '−' polarity. Based on this modal identification is done, and the observed resonant modes in RMSA are TM_{10}, TM_{02}, TM_{12}, TM_{22}, and TM_{30}. For the desired

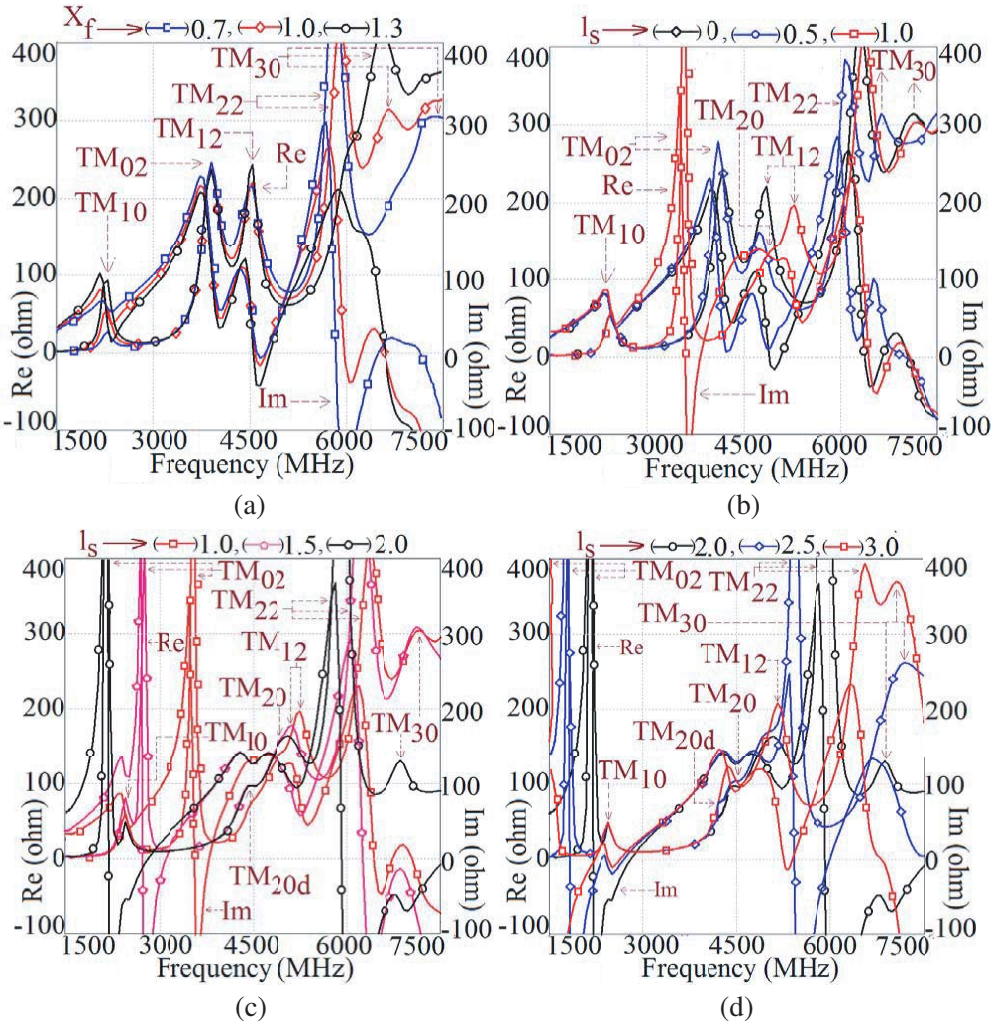

Figure 2. Resonance curve plots for (a) feed point and (b)–(d) slot length 'l_s' variations for the dual band E-shape MSA.

dual frequency response, each band should exhibit a similar radiation pattern. In RMSA, the radiation pattern at TM_{10} mode is broadside with lower cross polarization levels. At TM_{02} mode, it is conical or end-fire. The radiation pattern of TM_{12} mode is either conical or partially conical, which also depends upon the patch aspect ratio. A higher cross polar component is present at TM_{12} mode. It is reported in the literature that the introduction of a slot alters the current distribution at higher order modes which modifies their radiation pattern [24]. Therefore for analyzing the slot effects, parametric study is carried out for increments in slot lengths 'l_s', and corresponding resonance curve plots are as shown in Figs. 2(b)–(d). Also the modal surface current distributions observed at each peak for 'l_s' = 1.5 cm is as shown in Figs. 3(a)–(g).

In the current plots, the '+' and '−' signs represents the electric field polarity. The slot length is parallel to the current path at TM_{10} mode over a complete patch length; hence its frequency is unaffected against increment in slot length. Slot is placed parallel to the surface currents at TM_{20} and TM_{30} mode as well. But since they show two and three half wavelength variations along the complete patch length, variations in their frequencies are observed. When slots are allied orthogonal to surface current directions, they modify surface currents on the patch which reduces respective frequency. As slots are allied orthogonal to surface currents of TM_{02} mode, its frequency decreases drastically with incrementing slot lengths, and for 'l_s' = 2 cm onwards it goes below TM_{10} mode frequency. For slot length 'l_s' < 1.0 cm, TM_{12} and TM_{22} mode frequencies decrease due to the orthogonal orientation of

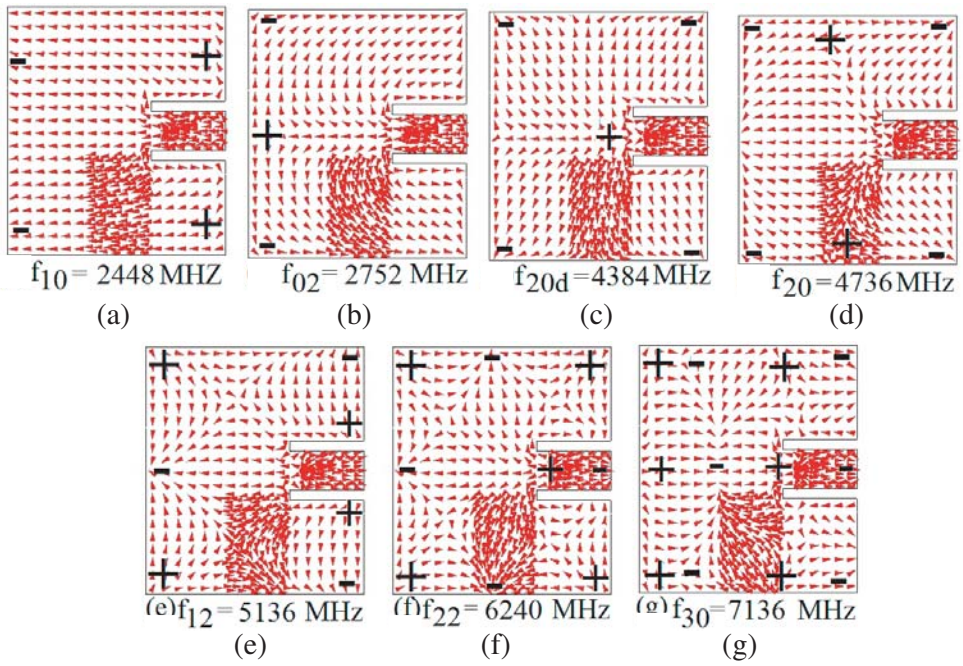

Figure 3. (a)–(g) Surface current distributions at observed resonant modes at 'l_s' = 1.5 cm for dual band E-shape MSA.

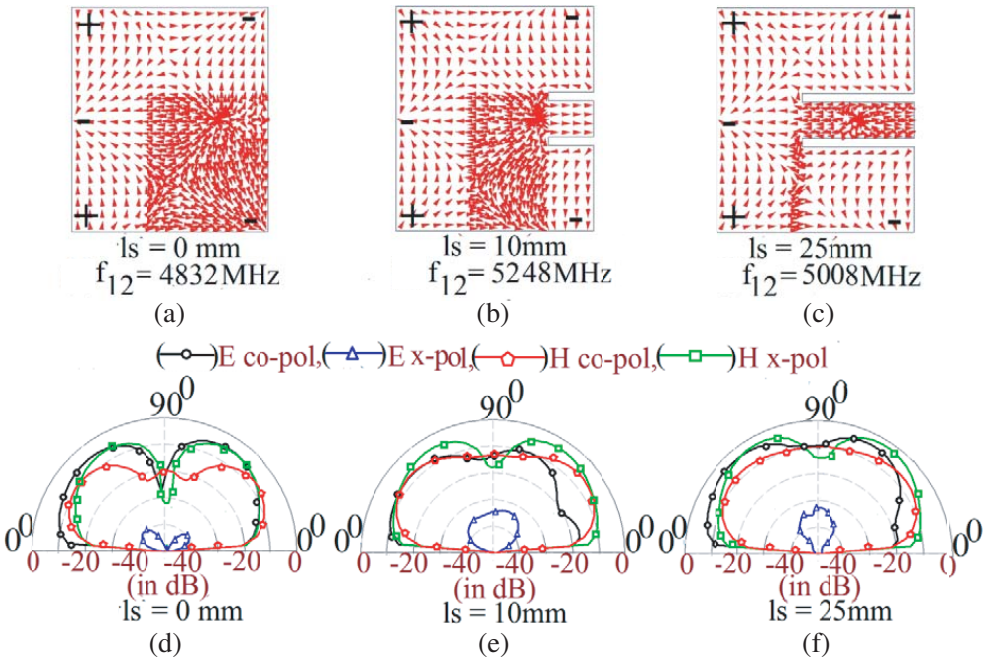

Figure 4. (a)–(c) Surface current distributions and (d)–(f) simulated radiation pattern plots at TM_{12} mode for different values of 'l_s' for dual band E-shape MSA.

their current path length with respect to the slot length along the patch width. But for 'l_s' $\geq$ 1.0 cm, effective patch width as seen by the coaxial feed for these two modes decreases, hence their frequencies increase. The radiation pattern at TM_{12} mode in RMSA is partially conical. Variation in slot length reorients the current distributions at TM_{12} mode. Due to this, the conical radiation pattern at TM_{12} mode is modified to broadside radiation pattern as shown in Figs. 4(a)–(f).

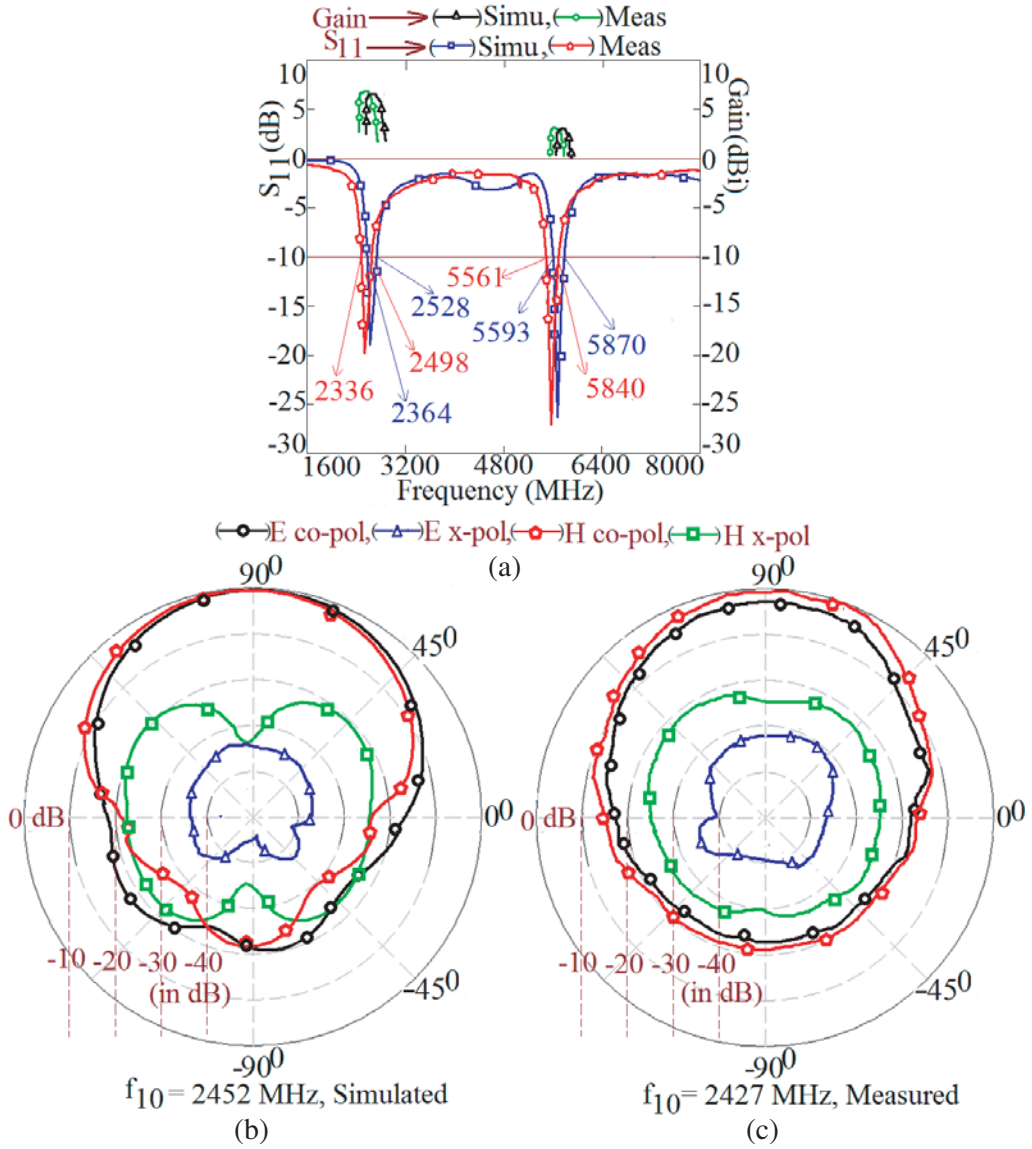

Figure 5. (a) Return loss and gain plots and (b), (c) radiation pattern at the first frequency of dual band response for dual band E-shape MSA.

The TM_{20} mode is observed for 'l_s' = 1.0 cm. For 'l_s' > 1.0 cm, one more weakly excited mode is observed prior to the TM_{20} mode. It shows similar two half wave length variations along the length just like TM_{20} mode. But these current variations are present from the patch center and towards the patch diagonal points as shown in Fig. 3(c). Hence this mode is referred to as TM_{20d} mode. Here 'd' stands for the diagonal variation. For 'l_s' in the range of 2.5 to 3.0 cm, proper impedance matching is observed for TM_{10} and TM_{12} modes showing frequency ratio in the range of 1 : 2.4 which is the required condition for the dual band design for WLAN. For 'l_s' $\geq$ 3.0 cm, impedances at all modes increase drastically due to effective reduction in patch width as seen by the modal currents. Hence 'l_s' = 2.6 cm is selected for the optimum dual band design. For the optimized dual band configuration, dimensions of E-shape MSA are 'L' = 4.2, 'W' = 5.0, 'l_s' = 2.6, 'w_s' = 2, 'Y_s' = 1.0, 'X_f' = 1.0 cm. The optimized configuration is fabricated on an air suspended low cost FR4 substrate and tested on a finite ground plane of size 10 × 10 cm. Measured and simulated return loss (S_{11}) and gain plots are as shown in Fig. 5(a).

The S_{11} plot indicates return loss for less than −10 dB in the two bands. The simulated frequencies and their respective BWs are 2452 and 5762 MHz and 164 (67%) and 246 MHz (4.2%). Corresponding

measured values are 2427 and 5730 MHz with a BW of 162 (6.6%) and 279 MHz (4.8%), respectively. Simulated broadside gains observed at respective bands are 6.7 and 2.3 dBi while measured values are 6.8 and 2.1 dBi. The ratio between dual frequencies is around 1 : 2.4, which is required in the WLAN application. The simulated and measured radiation patterns observed at the two frequencies are shown in Figs. 5(b), (c) and 6(a), (b). At both the frequencies, i.e., 'f_1' (TM_{10}) and 'f_2' (TM_{12}), broadside radiation pattern is observed with E-plane aligned along $\Phi = 0°$. A higher cross polarization level is observed in the H-plane at the second frequency. This may not be a disadvantage for indoor wireless communication applications where due to multiple reflections incident wave polarization is not fixed, and higher cross polar level antenna able to receive signal from any field orientation will reduce the signal loss. The deviation in the measurement results from the simulation results is attributed to the variation in substrate parameters, feed point location, as well as marginal error caused in the radiation pattern measurement setup. The same was carried out inside the antenna lab, wherein minimum reflections from the surrounding objects were ensured at the two frequencies. The fabricated antenna is as shown in Figs. 6(c), (d). Further in the paper, based upon the proposed optimum design, simpler parametric formulations for various antenna parameters are presented. They will be useful in the redesigning of a similar dual band configuration at given TM_{10} mode frequency and frequency ratio around 1 : 2.4.

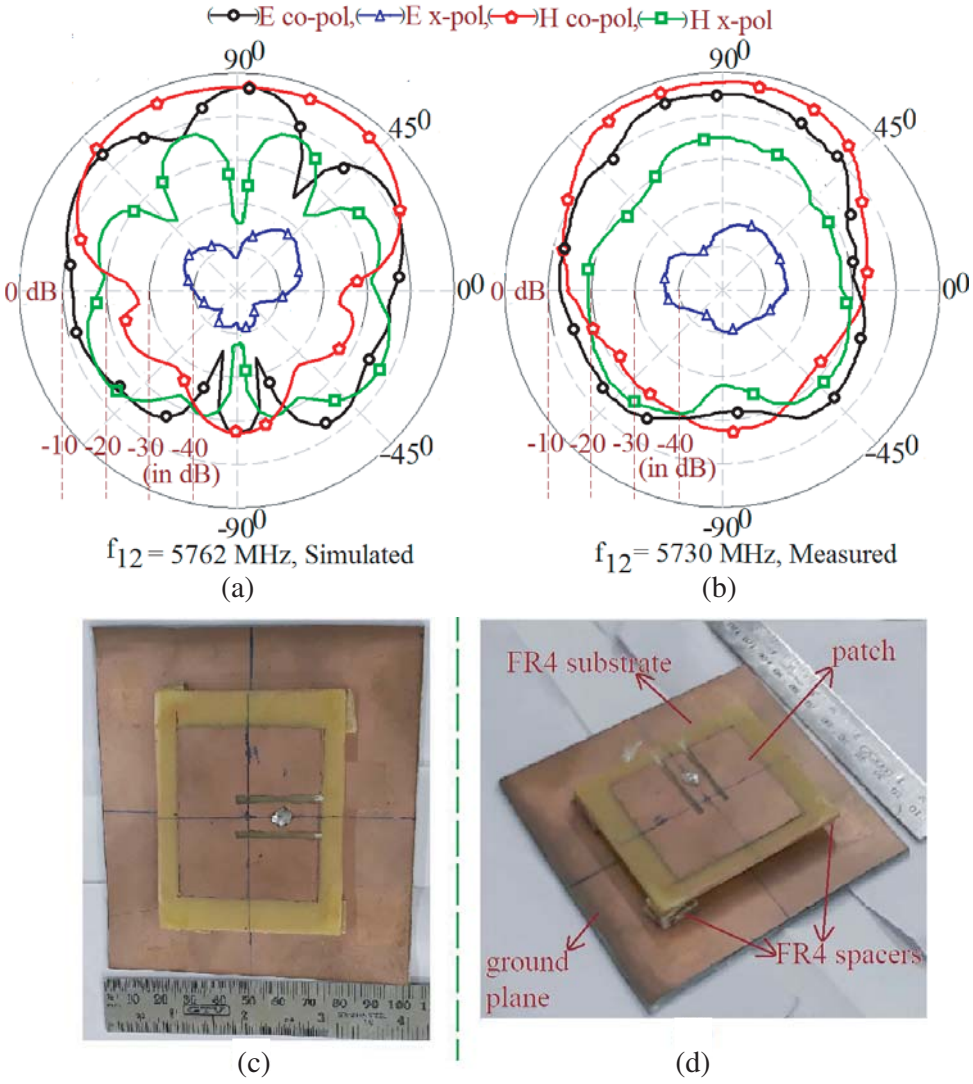

Figure 6. (a), (b) Radiation pattern at second frequency of the dual band response and (c) top and (d) 3D views of the fabricated antenna for dual band E-shape MSA.

3. DESIGN METHODOLOGY FOR DUAL BAND E-SHAPE MSA

The redesigning procedure proposed here is based upon the parametric study and subsequent optimum design discussed above. As the design uses suspended dielectric, value of effective dielectric constant (ε_{re}) needs to be calculated which decides the patch dimensions. Here the value of 'h_a' is not known. As the redesigned configuration is presented for a similar thinner substrate ($0.043\lambda_g$), for the initial calculation, the value of 'ε_{re}' is assumed to be 1.06. For the desired TM_{10} mode frequency (specified in GHz), the value of 'λ_g' is calculated in cm, using Equation (1). The total substrate thickness 'h_t' for the redesigned antenna is taken as '$0.043\lambda_g$' which equals '$h_a + h$'. Further practically realizable value of 'h_a' is selected, by which the values of 'ε_{re}' and 'λ_g' are recalculated using Equations (2) and (1), respectively. Again here the total substrate thickness is calculated as $0.043\lambda_g$. Using this, a new value of 'h_a' is found. It is observed in this iterative process that the value of practically realizable 'h_a' marginally changes with respect to the earlier value calculated. Hence the value of 'h_a' as calculated initially is maintained. The RMSA length 'L' for the given TM_{10} mode is calculated using Equation (3). With reference to the TM_{10} mode frequency, frequencies of other higher order orthogonal modes are decided by the patch aspect ratio 'L/W'. To maintain the same separation between the fundamental and various higher mode frequencies, patch width 'W' is taken as $1.19L$. Further, various other E-shape antenna parameters are calculated as, 'l_s' $= 0.232\lambda_g$, 'w_s' $= 0.0178\lambda_g$, 'Y_s' $= 0.0445\lambda_g$, 'X_f' $= 0.089\lambda_g$. These parameters are selected based upon their optimum antenna parameters as presented in the above design and expressed in terms of operating TM_{10} mode wavelength 'λ_g'. The dual band E-shape MSA is designed using these parametric formulations at three different TM_{10} mode frequencies. The redesigned antennas were simulated, and the experimentation was done for result verification. Various antenna parameters for the redesigned configurations are provided in Table 1. Their simulated and measured S_{11} and gain plots are shown in Figs. 7(a)–(c). In all the redesigned configurations, similar results to that observed in the proposed configuration with frequency ratio of around 1 : 2.4 are obtained. Thus given procedure can be used to redesign a similar dual band E-shape MSA at given TM_{10} mode frequency

$$\lambda_g = \frac{30}{f_{\mathrm{TM}_{10}}\sqrt{\varepsilon_{re}}} \tag{1}$$

$$\varepsilon_{re} = \frac{\varepsilon_r(h + h_a)}{(\varepsilon_r h_a + h)} \tag{2}$$

Table 1. Antenna parameters for the redesigned dual band E-shape MSAs.

Antenna Parameters	$\mathbf{f_{TM1,0} = 900\,MHz}$		$\mathbf{f_{TM1,0} = 1500\,MHz}$		$\mathbf{f_{TM1,0} = 1800\,MHz}$	
L	12.56 cm		7.36 cm		5.96 cm	
W	14.94 cm		8.75 cm		7.09 cm	
l_s	8.69 cm		4.72 cm		3.82 cm	
w_s	5.58 cm		0.34 cm		0.28 cm	
Ys	1.39 cm		0.81 cm		0.66 cm	
X_f	2.98 cm		1.75 cm		1.41 cm	
f_1	**Simulated**	**Measured**	**Simulated**	**Measured**	**Simulated**	**Measured**
	930 MHz	898 MHz	1520 MHz	1485 MHz	1808 MHz	1763 MHz
Bandwidth for f_1	70 MHz	62 MHz	110 MHz	102 MHz	120 MHz	105 MHz
Gain for f_1	6.8 dBi	6.5 dBi	6.7 dBi	6.5 dBi	6.8 dBi	6.7 dBi
f_2	2235 MHz	2225 MHz	3620 MHz	3575 MHz	4432 MHz	4392 MHz
Bandwidth for f_2	45 MHz	35 MHz	105 MHz	98 MHz	124 MHz	111 MHz
Gain for f_2	1.8 dBi	1.7 dBi	2 dBi	1.9 dBi	2.6 dBi	2.4 dBi

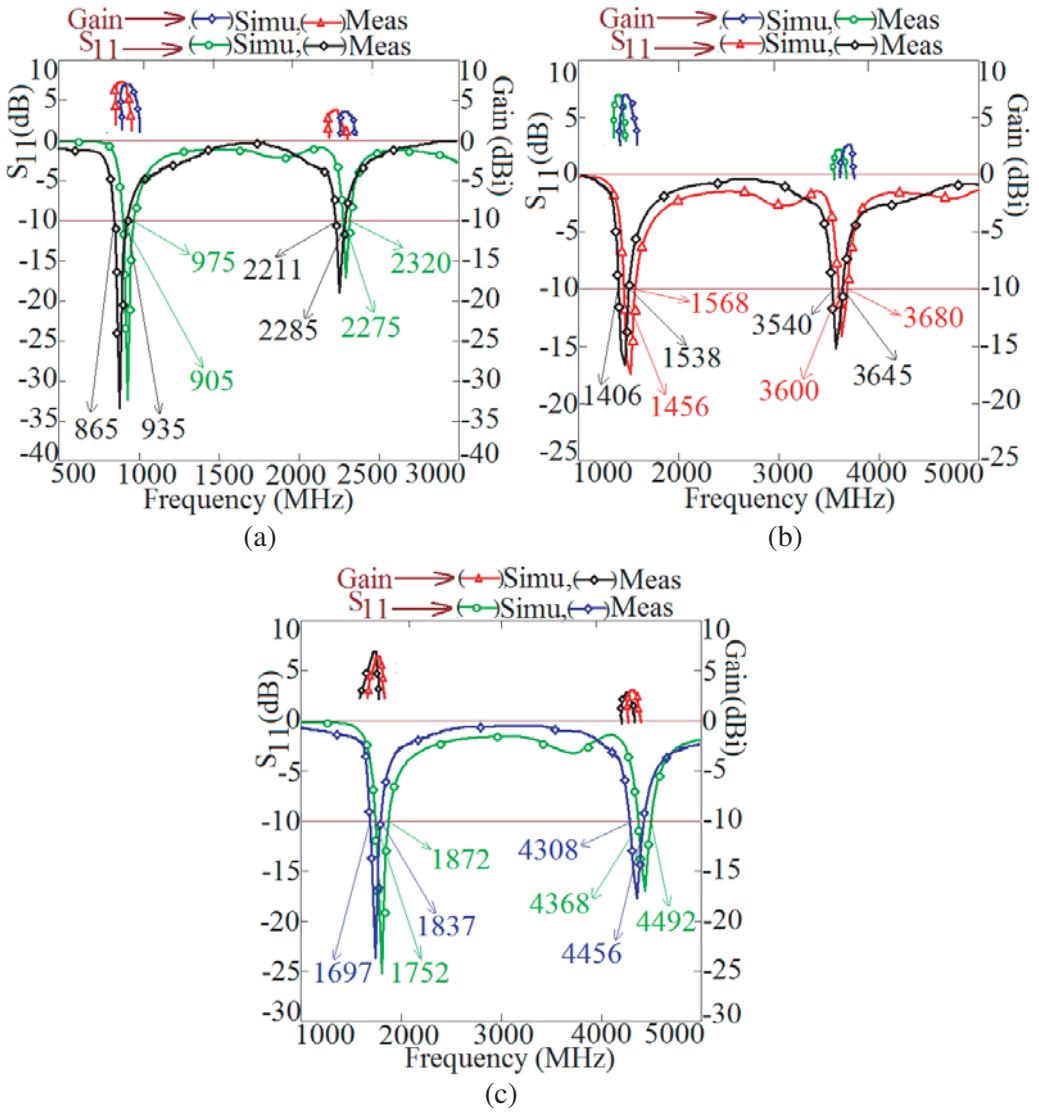

Figure 7. Return loss and Gain plots for the redesigned dual band E-shape MSA at (a) 900 MHz, (b) 1500 MHz, and (c) 1800 MHz.

$$L_p = \frac{30}{2f_{\mathrm{TM}_{10}}\sqrt{\varepsilon_{re}}} - 1.2\,(h + h_a) \tag{3}$$

A comparison between the proposed dual band E-shape MSA against the reported designs is given in Table 2. A dual frequency configuration reported in [11] though it is fabricated on electrically thicker substrate yields lesser BW against the proposed configuration which is fabricated on an electrically thinner substrate. Dual band operation is realized using L shape slots in [12, 13]. For the BW enhancement organic magnetic material is used for the substrate in [12], while the proposed configuration is fabricated on an air suspended low cost FR4. Owing to the complex feeding methods used in [14, 15], the proposed configuration uses a simpler coaxial feeding technique. A shorting pin with two pairs of rectangular slots is used in [16] while a rectangular loop with an E-shape patch with a shorting pin is used in [18]. Also an M-shape patch with shorting vias is used in [17] for the realization of dual band response with enhanced BW using an electrically thinner substrate. But these designs lack in depth explanations about patch modes with respect to shorting vias and embedded slots dimensions and positions, which is needed for in depth understanding of the antenna working. Against this proposed work provides in depth analysis explaining the effect of substrate thickness and slot on the multiband response with respect

Table 2. Comparison for the proposed dual band E-shape MSA against reported dual band MSAs.

MSA shown in	Meas. Freq., % and BW (MHz, %)	Frequency ratio $f2/f1$	Frequency tuning element	Peak Gain (dBi)	Patch area and substrate thickness (A/λ_c, h/λ_c)
Figs. 1(a), (b)	2427 (6.6), 5730 (4.8)	2.36	Slot	6.8, 2.1	$1.57\lambda_c$, $0.043\lambda_c$
Ref. [11]	2440 (4.13), 5250 (3.8)	2.15	slot	2.9, 1.9	$1.6\lambda_c$, $0.06\lambda_c$
Ref. [12]	2400 (3.3), 5200 (8.8)	2.16	slot	3.8, 5.8	$0.87\lambda_c$, $0.036\lambda_c$
Ref. [13]	2450 (4.13), 5125 (8.82)	2.09	slot	3.9, 8	$0.87\lambda_c$, $0.036\lambda_c$
Ref. [14]	2450 (4.6), 5500 (12.9)	2.24	slot	2.5, 4.3	$0.8\lambda_c$, $0.014\lambda_c$
Ref. [15]	2430 (4.9), 5760 (7.29)	2.37		10.17	$1.104\lambda_c$, $0.061\lambda_c$
Ref. [16]	2450 (3.7), 5200 (5.3)	2.12	slits	4.1, 1.4	$0.4\lambda_c$, $0.035\lambda_c$
Ref. [17] (dual band configuration)	2440 (0.5), 5770 (6)	2.36	–	4.96, 7.57	$3.4\lambda_c$, 0.024
Ref. [18]	2400 (3), 5500 (13)	2.29	slot	9.23, 6	$2\lambda_c$, $0.03\lambda_c$
Ref. [19]	Single band tuning range 5400–2400 (2.5% and 8%)	Tuning range 2.25 : 1	Capacitor and PIN diode	5.8	$1.18\lambda_c$, $0.013\lambda_c$
Ref. [20]	2400 (0.62), 5600 (1.6)	2.33	PIN diode	7	$2.05\lambda_c$, $0.009\lambda_c$
Ref. [21] (uniform width configuration)	2.43 (1.48), 5.43 (2.65)	2.23	–	4.8	$1.05\lambda_c$, $0.031\lambda_c$
Ref. [22]	2.4 (Not specified) 5.5 (Not specified)	2.29	–	5, 3.7	$1.13\lambda_c$, $0.045\lambda_c$

to patch modes. For the tuning of dual band operation pin diodes are used in [19, 20]. Against them, the proposed design yields frequency variation by changing the slots' dimensions for the individual patch modes. The uniform square ring configuration used for the realization of dual band response reported in [21] makes the overall structure complex compared with the simple slot cut technique used in the proposed configuration. As against single patch used in proposed configuration multiple patches have been used in [22] for the realization of dual band response. In addition, all the above mentioned configurations do not provide in depth design guidelines for the redesigning of a similar type of antenna

in different frequency ranges, which is provided in the present work.

Thus in comparison with the reported work, this paper presents a simple coaxial feed traditional E-shape patch for dual band response with frequency ratio of around 1 : 2.4. None of the reported papers on traditional E-shape MSA has exploited the higher order mode frequency response with respect to the realization of a dual band antenna. Against it, the proposed work highlights the realization of dual band response with respect to variations in substrate thickness from the broadband configuration of E-shaped MSA. Further, parametric study is provided with respect to feed position and slot dimension for bringing out resonant mode based explanation for the realized dual band response offering similar radiation pattern characteristics. The configuration fabricated on an air suspended low cost FR4 substrate yields appreciable BWs of 6.6 and 4.8% and co-polar broadside gains of 6.8 to 2.1 dBi at the respective bands of frequencies. Also the proposed work provides a parametric redesigning procedure for the dual band response. Antennas designed using them yield similar characteristics with frequency ratio of nearly 1 : 24. These are all the new technical contributions in the proposed work against the reported dual band MSA papers.

4. CONCLUSIONS

Conventional broadband E-shape MSA is studied with respect to its higher order mode frequency response for exploring the dual frequency characteristics. The decrease in the air gap in the suspended design yields impedance matching for fundamental and higher order modes to give possible dual band response. The detailed parametric study reveals that dual band response is the result of optimum separation between TM_{10} and TM_{12} modes of the rectangular patch giving similar radiation pattern characteristics. The optimized configuration on thinner substrate ($0.043\lambda_g$) yields dual band response with resonance frequencies centered at 2427 and 5730 MHz with BWs of 6.6% and 4.8%, respectively. Broadside gains of 6.8 and 2.1 dBi are observed in the two bands. Thus, the design can entirely cover 2.4/5.8 GHz bands of WLAN applications. Redesigning guidelines are proposed based on the parametric analysis done. The antenna designed using the proposed guidelines yields a similar dual band response with the frequency ratio of 1 : 2.4 showing similar radiation pattern characteristics in the two bands.

REFERENCES

1. Wong, K. L., *Compact and Broadband Microstrip Antennas*, 1st edition, John Wiley & Sons, Inc., New York, USA, 2002.
2. Kumar, G. and K. P. Ray, *Broadband Microstrip Antennas*, 1st edition, Artech House, USA, 2003.
3. Balanis, C. A., *Antenna Theory & Design*, 3rd edition, John Wiley & Sons Inc. Publication, 2005.
4. Garg, R., P. Bhartia, and I. Bahl, *Microstrip Antenna Design Handbook*, Artech House, London, 2001.
5. Anasri, J. A., S. K. Dubey, P. Singh, R. U. Khan, and B. R. Vishvakarma, "Analysis of U-slot loaded patch for dual band operation," *International Journal of Microwave and Optical Technology*, Vol. 3, 80–84, 2008.
6. Sheta, A. F., A. Mohra, and S. F. Mahmoud, "Multi-band operation of a compact H-shaped microstrip antenna," *Microwave and Optical Technology Letters*, Vol. 35, No. 5, 363–367, 2002.
7. Shynu, S. V., G. Augustin, C. K. Aanandan, P. Mohanan and K. Vasudevan, "C-shaped slot loaded reconfigurable microstrip antenna," *Electronics Letters*, Vol. 42, 316–317, 2006.
8. Liu, S., S.-S. Qi, W. Wu, and D.-G. Fang, "Singlelayer single patch four band asymmetrical U-slot patch antenna," *IEEE Transaction on Antennas and Propagation*, Vol. 62, No. 9, 4895–4899, 2014.
9. Gulam Nabi Alsath, M. and M. Kanagasabai, "Planar penta-band antenna for vehicular communication application," *IEEE Antennas Wireless Propagation Letters*, Vol. 13, 110–113, 2014.
10. Wong, K.-L. and S.-T. Fang, "Reduced-size circular microstrip antenna with dual-frequency operation," *Microwave and Optical Technology Letters*, Vol. 18, 54–56, 1998.

11. Zhong, Q., Y. Li, H. Jiang, and Y. Long, "Design of a novel dual-frequency microstrip patch antenna for WLAN applications," *IEEE Antennas and Propagation Society International Symposium*, Vol. 1, 277–280, 2004.
12. Wang, E., J. Zheng, and Y. Liu, "A novel dual-band patch antenna for WLAN communication," *Progress In Electromagnetic Research C*, Vol. 6, 93–102, 2010.
13. Mishra, A., J. A. Ansari, K. Kamakshi, A. Singh, Mohd. Aneesh, and B. R. Vishwakarma, "Compact dual-band rectangular microstrip patch antenna for 2.4/5.12 GHz wireless applications," *Wireless Networks*, Vol. 21, No. 2, 347–355, 2014.
14. Xi, D., L. H. Wen, Y. Z. Yin, Z. Zhang, and Y. N. Mo, "A compact dual inverted C-shaped slots antenna for WLAN applications," *Progress In Electromagnetic Research Letters*, Vol. 17, 115–123, 2010.
15. Mobashsher, A. T., M. T. Islam, and N. Misran, "A novel high-gain dual-band antenna for RFID reader applications," *IEEE Antennas Wireless Propagation Letters*, Vol. 9, 653–656, 2010.
16. Tung, H. C. and K. L. Wong, "A shorted microstrip antenna for 2.4/5.2 GHz dual-band operation," *Microwave Optical Technology Letters*, Vol. 30, 401–402, 2001.
17. Peng, L., C.-L. Ruan, and X.-H. Wu, "Design and operation of dual/triple-band asymmetric M-shaped microstrip patch antennas," *IEEE Transaction on Antennas and Propagation*, Vol. 10, 1069–1072, 2010.
18. Meng, F. and S. Sharma, "A single feed dual-band (2.4 GHz/5 GHz) miniaturized patch antenna for wireless local area network (WLAN) communications," *Journal of Electromagnetic Waves and Applications*, Vol. 30, No. 18, 2390–2402, 2016.
19. Abdulraheem, Y. I., G. A. Oguntala, A. S. Abdullah, H. J. Mohammed, R. A. Ali, R. A. Abd-Alhameed, and J. M. Noras, "Design of frequency reconfigurable multiband compact antenna using two PIN diodes for WLAN/WiMAX applications," *IET Microwaves, Antennas & Propagation*, Vol. 11, No. 8, 1098–1105, 2017.
20. Tekin, I. and M. Knox, "Reconfigurable microstrip patch antenna for WLAN software defined radio applications," *Microwave Optical Technology Letters*, Vol. 54, 644–649, 2012.
21. Behera, S. and K. J. Vinoy, "Microstrip square ring antenna for dual band operation," *Progress In Electromagnetics Research*, Vol. 93, 41–56, 2009.
22. Jung, C. W. and F. De Flaviis, "A dual-band antenna for WLAN applications by double rectangular patch with 4-bridges," *IEEE Antennas and Propagation Society International Symposium*, Vol. 4, 4280–4283, 2004.
23. CST Microwave Studio, Version 2019.
24. Deshmukh, A. A. and K. P. Rayand Ameya Kadam, "Analysis of slot cut broadband and dual band rectangular microstrip antennas," *IETE Journal of Research*, Vol. 59, No. 3, 193–200, 2013.